Supplementary Material

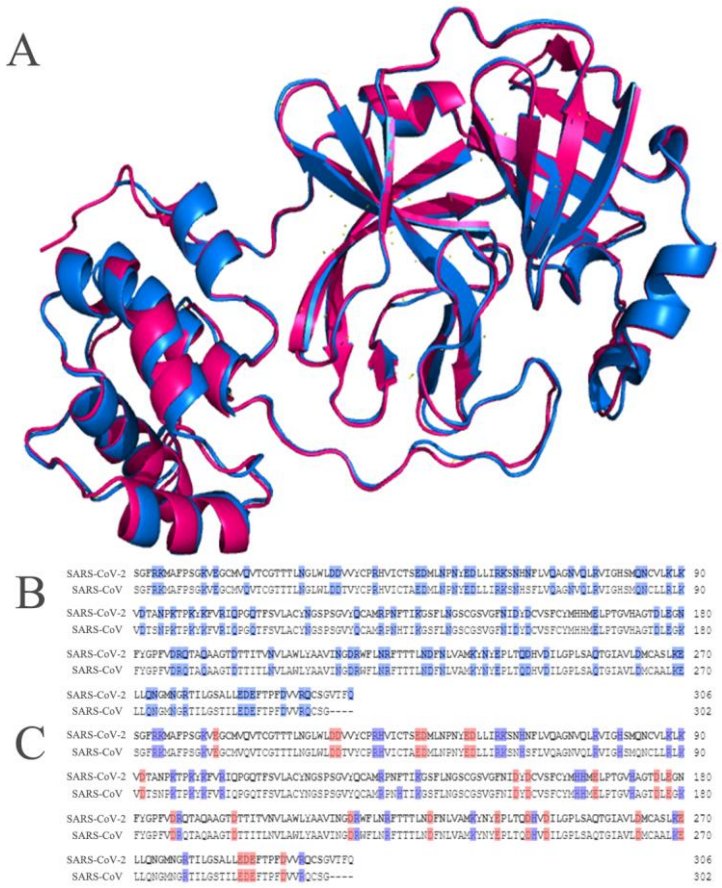

Figure S1: 3CL^{pro} amino acid sequence and structure analysis. (A) A comparison of two 3CL^{pro} structures of SARS-CoV and SARS-CoV-2. 3CL^{pro} of SARS-CoV （2Z9J）was shown in blue, and 3CL^{pro} of SARS-CoV-2（6LU7）was shown in red. (B) The 3CL^{pro} amino acid sequences of both SARS-Cov and SARS-CoV-2 were compared, and the polar amino acids were marked in blue. (C) Comparison of the 3CL^{pro} amino acid sequence of both SARS-Cov and SARS-CoV-2. Negatively charged amino acids were shown in red and positively charged amino acids are shown in red.

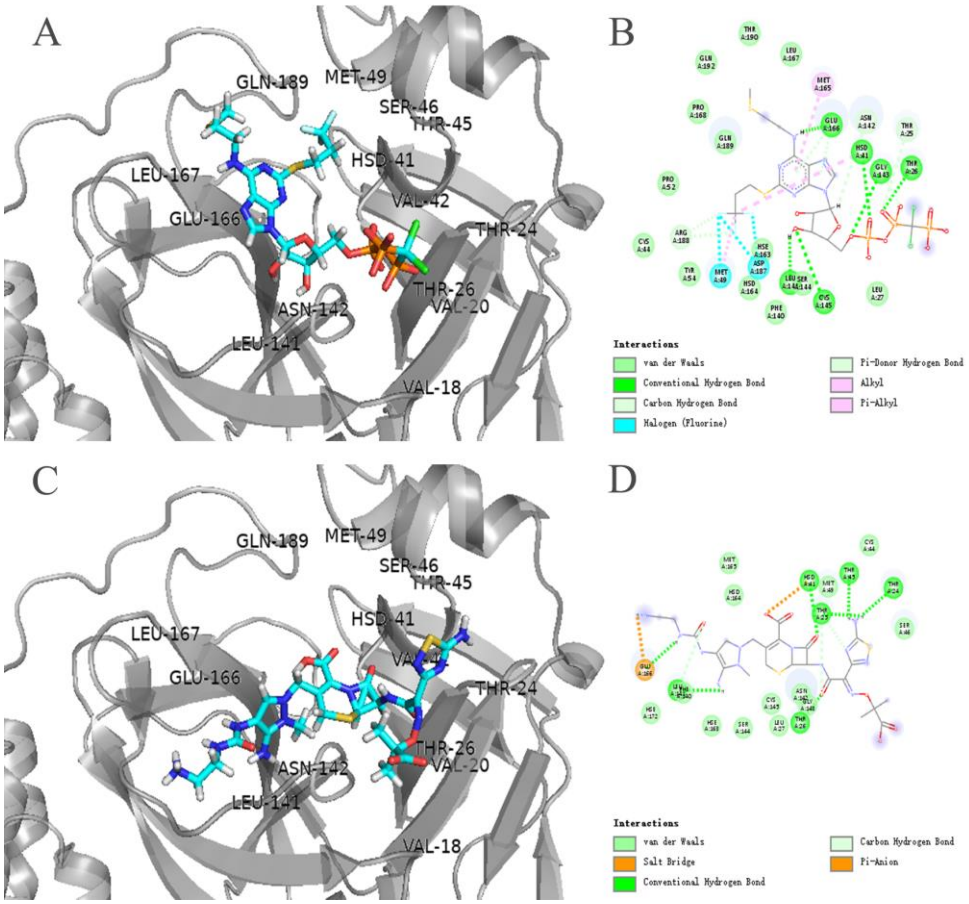

Figure S2: Three-dimensional binding modes of Cangrelor and Ceftolozane with $3CL^{pro}$. (A and C) The three-dimensional binding modes of both Cangrelor and Ceftolozane with $3CL^{pro}$, respectively Protein shown as a cartoon model and ligands shown as stick model. (B and D) The interaction modes of both Cangrelor and Ceftolozane with $3CL^{pro}$, respectively.

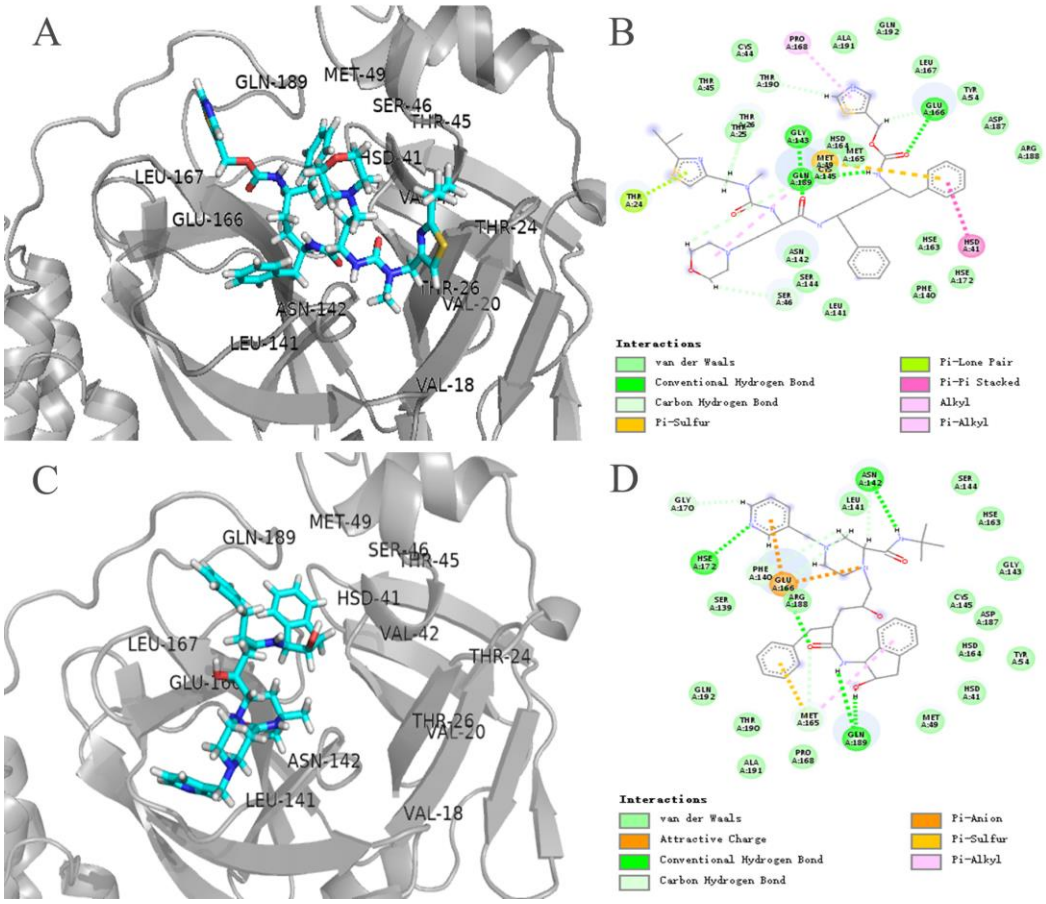

Figure S3: Three-dimensional binding modes of Cobicistat and Indinavir with $3CL^{pro}$. (A and C) The three-dimensional binding modes of both Cobicistat and Indinavir with $3CL^{pro}$, respectively. Protein shown as a cartoon model and ligands shown as stick model. (B and D) The interaction modes of both Cobicistat and Indinavir with $3CL^{pro}$, respectively.

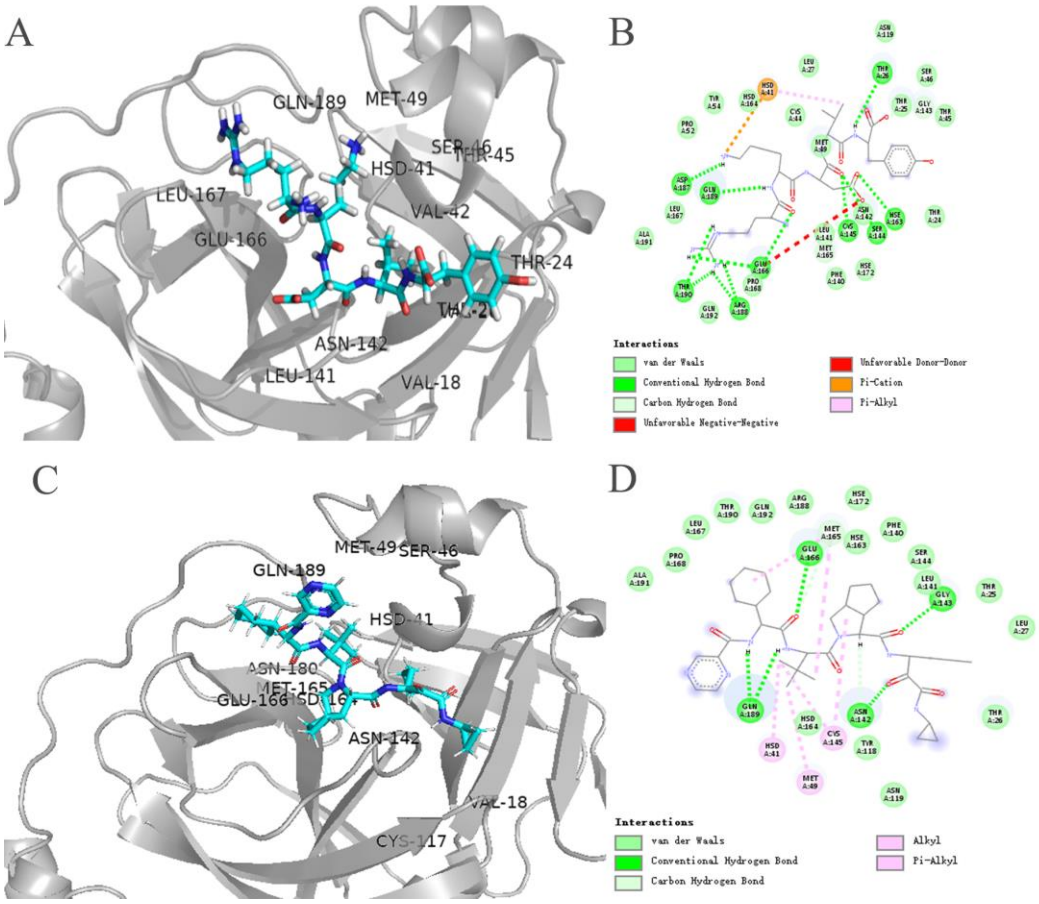

Figure S4: Three-dimensional binding modes of Thymopentin and Telaprevir with $3CL^{pro}$. (A and C) The three-dimensional binding modes of both Thymopentin and Telaprevir with $3CL^{pro}$, respectively. Protein shown as a cartoon model and ligands shown as stick model. (B and D) The interaction modes of both Thymopentin and Telaprevir with $3CL^{pro}$, respectively.

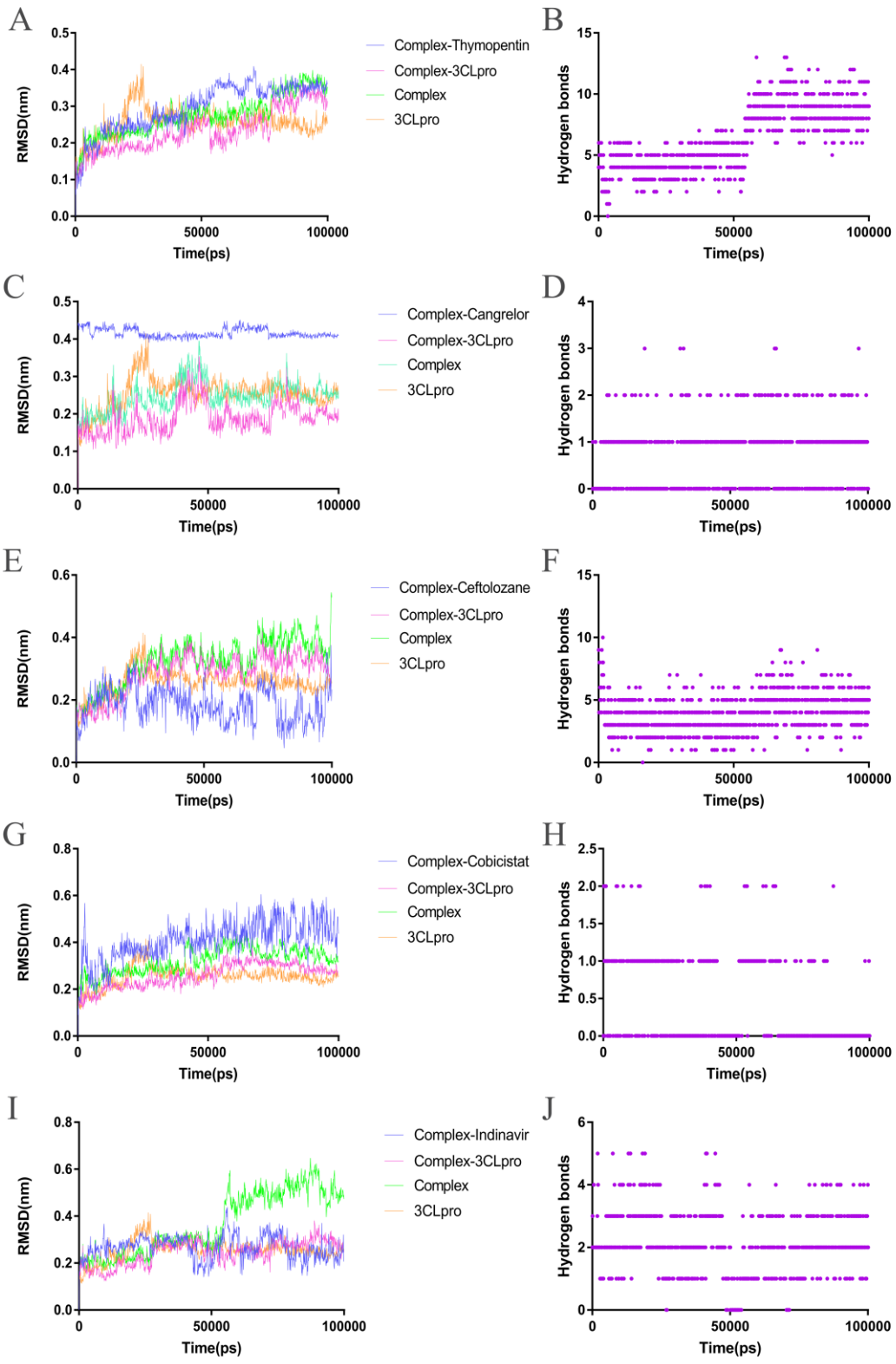

Figure S5: Analysis of Molecular Dynamics Simulation results of the free $3CL^{pro}$ and the $3CL^{pro}$-drug complex. (A) Root Mean Square Deviation (RMSD) of the $3CL^{pro}$-Thymopentin complex and the free $3CL^{pro}$. (B) Intermolecular hydrogen

bonds between the Thymopentin and the $3CL^{pro}$. (C) RMSD of the $3CL^{pro}$-Cangrelor complex and the free $3CL^{pro}$. (D) Intermolecular hydrogen bonds between the Cangrelor and $3CL^{pro}$. (E) RMSD of the $3CL^{pro}$-Ceftolozane complex and the free $3CL^{pro}$. (F) Intermolecular hydrogen bonds between the Ceftolozane and $3CL^{pro}$. (G) RMSD of the $3CL^{pro}$-Cobicistat complex and the free $3CL^{pro}$. (H) Intermolecular hydrogen bonds between the Cobicistat and $3CL^{pro}$. (G) RMSD of the $3CL^{pro}$-Indinavir complex and the free $3CL^{pro}$. (H) Intermolecular hydrogen bonds between the Indinavir and $3CL^{pro}$.

Movie 1: Molecular dynamics simulation of the docking complex of Viomycin and $3CL^{pro}$. Surface represents $3CL^{pro}$, and sticks represent Viomycin.

Movie 2: Molecular dynamics simulation of the docking complex of Capastat and $3CL^{pro}$. Surface represents $3CL^{pro}$, and sticks represent Ritonavir.

Movie 3: Molecular dynamics simulation of the docking complex of Ritonavir and $3CL^{pro}$. Surface represents $3CL^{pro}$, and sticks represent Ritonavir.

Movie 4: Molecular dynamics simulation of the docking complex of Lopinavir and $3CL^{pro}$. Surface represents $3CL^{pro}$, and sticks represent Lopinavir.

Movie 5: Molecular dynamics simulation of the docking complex of Carfilzomib and $3CL^{pro}$. Surface represents $3CL^{pro}$, and sticks represent Carfilzomib.

Movie 6: Molecular dynamics simulation of the docking complex of Saquinavir and $3CL^{pro}$. Surface represents $3CL^{pro}$, and sticks represent Saquinavir.